

Radiative Model of Neutrino Mass with Neutrino Interacting MeV Dark Matter

Abdesslam Arhrib¹, Céline Boehm², Ernest Ma³ and Tzu-Chiang Yuan^{4,5}

¹*Département de Mathématique, Faculté des Sciences et Techniques,
Université Abdelmalek Essaadi, B. 416, Tangier, Morocco*

²*LAPTH, UMR 5108, 9 chemin de Bellevue - BP 110, 74941 Annecy-Le-Vieux, France*

³*Department of Physics and Astronomy,
University of California, Riverside, California 92521, USA*

⁴*Institute of Physics, Academia Sinica, Nangang, Taipei 11529, Taiwan*

⁵*Physics Division, National Center for Theoretical Sciences, Hsinchu, Taiwan*

Abstract

We consider the radiative generation of neutrino mass through the interactions of neutrinos with MeV dark matter. We construct a realistic renormalizable model with one scalar doublet (in addition to the standard model doublet) and one complex singlet together with three light singlet Majorana fermions, all transforming under a dark $U(1)_D$ symmetry which breaks softly to Z_2 . We study in detail the scalar sector which supports this specific scenario and its rich phenomenology.

1 Introduction

The nature of dark matter (DM) is one of the most disputed topics in cosmology. Until one (or two) decade(s) ago, only a few candidates prevailed in the literature, among which were neutralinos (a thermal, cold, DM species) and axions (also cold DM but non-thermal). Astrophysical and cosmological anomalies since in the last 10-15 years however led many authors to study more exotics scenarios, such as light DM, leptophilic DM, sterile neutrinos [1, 2, 3, 4, 5]. So far most DM studies have focused on either almost massless particles (axions), keV particles (sterile neutrinos) or GeV to TeV DM candidates (as provided by supersymmetry and Kaluza-Klein theories¹) but the range between a few keV and GeV has been somewhat disregarded.

In cosmology, both keV and GeV-TeV DM candidates are generally assumed to be collisionless, even though their annihilations or decay are invoked to explain the observed DM abundance. About a decade ago, it was pointed out that – even weak-strength – DM interactions could erase the DM primordial interactions and should not be disregarded when the DM is relatively light (a few MeV) and coupled to neutrinos or photons [7, 8]. Indeed the damping of the DM primordial fluctuations has two origins, as shown in these references: one is the collisional damping, which suppresses the matter fluctuations until the DM is kinetically decoupled from any other species; this is analogous to the Silk damping. The other source is the DM free-streaming which erases fluctuations that have not been erased yet by the DM collisions.

The resulting linear matter power spectrum associated with light DM candidates coupled to radiation features damped oscillations in addition to an exponential cut-off [9, 10, 11]. This makes these scenarios interesting alternatives to vanilla CDM and Warm DM candidates.

¹For a review see Ref. [6].

There has been much interest in the DM-neutrino coupling since these first studies but with the twist of DM self-interactions [12, 13, 14, 15]. However, as shown in Refs. [16, 17, 18], a sole DM-neutrino coupling can solve the missing satellite (which is a deficit of dwarf galaxy haloes in Milky Way-like DM haloes) and the too big to fail problems when the DM elastic scattering off neutrinos is of the order of

$$\sigma_{\text{el}} \simeq 10^{-36} \left(\frac{m_{\text{DM}}}{\text{MeV}} \right) \text{ cm}^2. \quad (1)$$

For DM candidates with a mass of about a few MeV, these interactions are typically of the order of the Standard Model weak interactions. Assuming a simple crossing between the elastic scattering and annihilations processes, one expects an annihilation cross section of the order of

$$\sigma v \simeq 3 \cdot 10^{-26} \left(\frac{m_{\text{DM}}}{\text{MeV}} \right) \text{ cm}^3/\text{s}, \quad (2)$$

which is the required value to explain the observed DM abundance in thermal DM scenarios. The correspondence between Eq. (1) and Eq. (2) thus suggests that current cosmological problems could be related to the current DM abundance.

Even more puzzling is the possibility to explain in some specific models [19, 20, 21] the existence of small neutrino masses in the presence of such a DM-neutrino coupling. It is therefore tempting to assume that there exists a framework in which DM-neutrino interactions can explain simultaneously the missing satellite and too big to fail problems, the existence of small neutrinos masses and the observed DM abundance.

In this paper we construct such a framework. We envision a fundamental Yukawa coupling of the form $\bar{N}_R \nu_L \zeta_2$ where the dark matter candidate, here referred to as N , is a Majorana fermion and both the fermion N and the scalar ζ_2 are light, with masses of order a few MeV. In Section 2, we review the elastic scattering cross section among the neutrino and DM and the related process of DM annihilation into neutrino pair based on this Yukawa

coupling. To support this specific scenario, we study an extension of the standard model with one additional scalar doublet and one additional complex singlet, both of which transform nontrivially under a dark global $U(1)_D$ that is softly broken into a discrete Z_2 (Section 3). We show how realistic neutrino masses may be obtained with a scalar mass spectrum including the light ζ_2 without conflicting with present data at the Large Hadron Collider (LHC) (Sections 3 and 4). We examine also in detail the scalar sector and obtain theoretical and phenomenological constraints on its parameter space (Section 4). Numerical results are presented in Section 5 and conclusion in Section 6. Some useful formulas are collected in the Appendix.

2 Elastic scattering and annihilation cross sections

In (thermal) scenarios where DM can scatter off neutrinos, the collisional damping scale is determined by the integral

$$l_{\text{coll damping}}^2 \simeq \int^{t_{\text{dec(DM}-\nu)}} \frac{\rho_\nu}{(\rho + p)_{\text{tot}} a^2 \Gamma_\nu} v^2 dt, \quad (3)$$

where a is the scale factor, ρ_ν the neutrino energy density, Γ_ν the neutrino interaction rate, v the neutrino velocity, $(\rho + p)_{\text{tot}}$ is the sum over the energy density and pressure of all the species coupled to the DM while DM still interacts with neutrinos (which includes the DM itself). This length is directly proportional to the neutrino density and velocity (which is equal to c if one assumes that the DM kinetic decoupling from neutrinos happens well before neutrinos become non relativistic) and the neutrino kinetic decoupling time [7, 8]. Its magnitude also depends on the period over which the DM is coupled to neutrinos; hence the integral over time, with $t_{\text{dec(DM}-\nu)}$ (the DM decoupling time from neutrino) as upper bound.

The CMB and linear matter power spectra in the presence of such a DM-neutrino coupling can be easily predicted using the Boltzmann formalism [11, 22]. Both agree with the damping

length estimate obtained analytically using the above formula (in the absence of mixed damping). But the matter power spectrum ultimately sets the stronger constraint, namely

$$\sigma_{\text{el}} = 10^{-36} \left(\frac{m_{\text{DM}}}{\text{MeV}} \right) \text{ cm}^2, \quad (4)$$

if the cross section is independent of the temperature or

$$\sigma_{\text{el}} = 10^{-48} \left(\frac{m_{\text{DM}}}{\text{MeV}} \right) \left(\frac{T}{2.7 \cdot 10^{-4} \text{ eV}} \right)^2 \text{ cm}^2, \quad (5)$$

if the cross section depends on the neutrino energy [22]. This confirms that a weak strength cross section can erase DM fluctuations at cosmologically relevant scales, if the DM is relatively light. The simplest elastic scattering process $N \nu \rightarrow N \nu$ that gives rise to such an effect relies on the exchange of a fermion (scalar) if the DM is a scalar (fermion). The cross section for a Majorana candidate coupled to neutrinos with a coupling g is given by the u and s-channels diagrams, leading to:

$$\sigma_{\text{el}} \simeq \frac{3}{16} \frac{g^4}{\pi} \frac{T^2}{(m_N^2 - m_{\zeta_2}^2)^2}, \quad (6)$$

in the absence of a close degeneracy between the mediator and DM masses. Here we also implicitly assume MeV DM, *i.e.* that DM is non relativistic at the DM-neutrino decoupling, which occurs slightly below a keV. The annihilation diagrams (t and u-channels) lead to the dominant contribution

$$\sigma v \simeq \frac{g^4}{4 \pi m_{\zeta_2}^2} \simeq 2.38 \cdot 10^{-26} \left(\frac{g}{4 \cdot 10^{-4}} \right)^4 \left(\frac{m_{\zeta_2}}{\text{MeV}} \right)^{-2} \text{ cm}^3/\text{s}, \quad (7)$$

where we again assume that there is not a strict degeneracy between the DM and mediator masses and neglect the neutrino mass.

Eqs. (6) and (7) cannot be satisfied simultaneously with the same values of the mass and couplings, unless the DM mass is slightly smaller than a few keV. Yet thermal keV annihilating DM particles into neutrinos are already ruled out [23, 24, 25, 26], as they would

change the number of relativistic degrees of freedom at nucleosynthesis and CMB time, by too large an amount. The only possibility for thermal DM candidates coupled to neutrinos is to have a mass above a few MeV [25].

In order to explain both the DM abundance and solve cosmological problems, one thus needs thus to get rid off the temperature dependence of the elastic scattering cross section. This occurs if the mass splitting between N and ζ_2 are of the order of a few keV or below. Indeed in this case the elastic scattering cross section reads

$$\sigma_{\text{el}} \simeq \frac{g^4}{16 \pi m_N^2} \simeq 10^{-36} \left(\frac{g}{6 \cdot 10^{-4}} \right)^4 \left(\frac{m_N}{\text{MeV}} \right)^{-2} \text{ cm}^2, \quad (8)$$

while the annihilation cross section is given by

$$\sigma v \simeq \frac{g^4 m_N^2}{4 \pi (m_{\zeta_2}^2 + m_N^2)^2} \simeq 3 \cdot 10^{-26} \left(\frac{g}{6 \cdot 10^{-4}} \right)^4 \left(\frac{m_N}{\text{MeV}} \right)^{-2} \text{ cm}^3/\text{s}. \quad (9)$$

Therefore, a scenario where the DM is of a few MeVs but the mediator is only slightly heavier than the DM by a few keVs can solve the missing satellite and too big to fail problems (in the absence of baryonic physics) and also explain the DM observed abundance.

Note that the presence of baryonic interactions could alter these values. Depending on the magnitude of the effect, one might either lose the above correspondence or be able to make a temperature dependent elastic scattering and temperature independent annihilation cross section compatible. Given that such studies do not exist yet, we will take the above numbers (see Eqs. (8) and (9)) at face value.

We now investigate whether such a scenario can also give rise to neutrino masses. Note that such a scenario predicts a slightly larger value of N_{eff} than 3.046 and $H_0 \simeq 71 \text{ km/s/Mpc}$ [22].

3 Radiative Neutrino Mass Through Dark Matter

The simplest finite one-loop radiative model of neutrino mass through dark matter is the scotogenic model (from the Greek “scotos” meaning darkness) proposed in 2006 [27]. It assumes an exactly conserved Z_2 symmetry [28] and extends the standard model (SM) of particle interactions with the addition of one scalar doublet (η^+, η^0) and three singlet Majorana fermions $N_{1,2,3}$ which are odd under Z_2 . Many aspects of its phenomenology have been studied in detail [29]. Whereas the masses of η and N are usually considered to be heavy, this mechanism also allows N to be light [30]. With the discovery [31, 32] of the 125 GeV particle at the Large Hadron Collider (LHC) and its identification with the long-sought Higgs boson h of the SM, important constraints on η are now applicable. From the limit on the invisible width of h , a light scalar (\sim MeV) is not allowed in the context of the original scotogenic model.

In this paper we consider the further addition of a complex scalar singlet χ and impose a dark $U(1)_D$ symmetry which is softly broken to Z_2 .

Whereas all SM fields have zero $U(1)_D$ charge, all other fields η , χ and $N_{1,2,3}$ are assumed to have the same nonzero $U(1)_D$ charge, say +1. To get the required neutrino mass and Higgs interaction, it does not work with just the inert Higgs doublet η , nor with the addition of a real scalar singlet. However, as shown in this paper, it will work with the η doublet plus a complex singlet χ , which is naturally maintained with a dark $U(1)_D$ symmetry, softly broken to Z_2 so that N may have a Majorana mass and ν gets a one-loop radiative mass as shown in Fig. 1. If only Z_2 is used, then many more allowed terms appear in the Lagrangian, such as $(\Phi^\dagger \Phi)\chi^2 + \text{H.c.}$ on top of $(\Phi^\dagger \Phi)\chi^* \chi$, which are unnecessary complications (and must indeed be small) in the subsequent discussion of the scalar sector.

The scalar potential is given by

$$\begin{aligned}
V = & m_1^2 \Phi^\dagger \Phi + m_2^2 \eta^\dagger \eta + m_3^2 \chi^* \chi + \frac{1}{2} m_4^2 [\chi^2 + (\chi^*)^2] \\
& + \mu [\eta^\dagger \Phi \chi + \Phi^\dagger \eta \chi^*] + \frac{1}{2} \lambda_1 (\Phi^\dagger \Phi)^2 + \frac{1}{2} \lambda_2 (\eta^\dagger \eta)^2 + \frac{1}{2} \lambda_3 (\chi^* \chi)^2 \\
& + \lambda_4 (\eta^\dagger \eta) (\Phi^\dagger \Phi) + \lambda_5 (\eta^\dagger \Phi) (\Phi^\dagger \eta) + \lambda_6 (\chi^* \chi) (\Phi^\dagger \Phi) + \lambda_7 (\chi^* \chi) (\eta^\dagger \eta) , \quad (10)
\end{aligned}$$

where the m_4^2 term breaks $U(1)_D$ softly to Z_2 . Note that the quartic term $(\Phi^\dagger \eta)^2$ present in the original Z_2 model [27] is now forbidden.

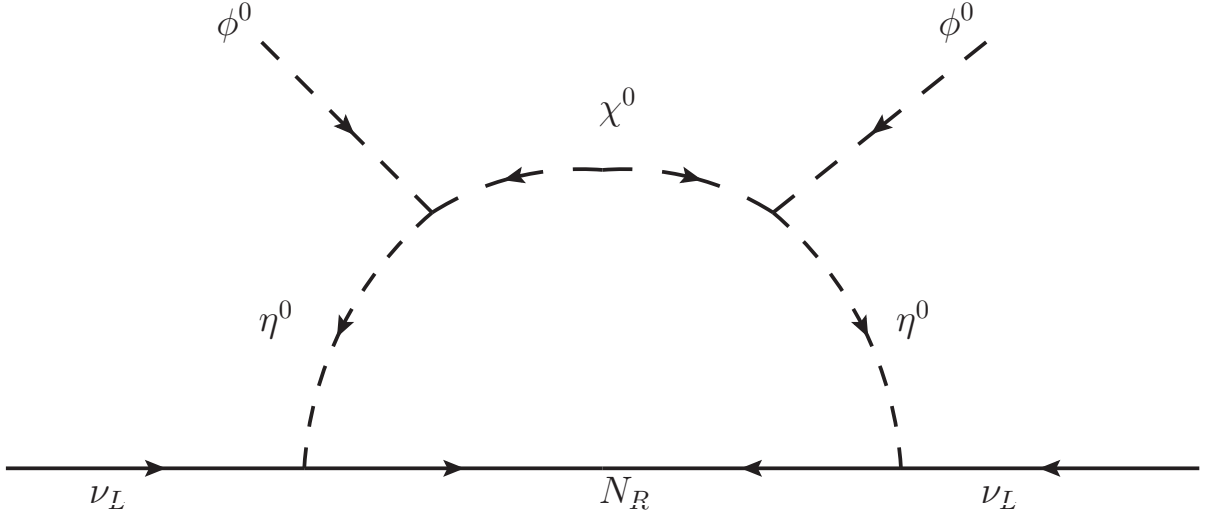


Figure 1: One-loop scotogenic neutrino mass from $U(1)_D$ breaking to Z_2 .

The one-loop mechanism for neutrino mass is depicted in Fig. 1, from which we can easily see that the Majorana mass term for N_i breaks $U(1)_D$ to Z_2 . This diagram is similar to that required in a supersymmetric extension [33]. We note that the m_4^2 and Majorana mass terms are the only two terms in the model that softly break $U(1)_D$ into Z_2 . This is a well-known method in symmetry breaking, because soft breaking generates only finite corrections in the renormalizable terms of the Lagrangian and a well-known rationale for setting m_4 small against other mass parameters (because its absence enlarges the symmetry of the theory). The model however remains renormalizable. These soft terms are analogous to the sfermion

mass and the gaugino mass in MSSM which break supersymmetry softly. The origin of these softly breaking terms may be revealed only at a higher theory. In the case of MSSM, these soft terms could arise from supergravity. In our case, we will treat them as phenomenological terms, just like the superpartner mass terms in MSSM, without worrying about the higher theory. For an early application of this idea in neutrino physics, see for example [34].

Let $\Phi = [\omega_1^+, (v + \phi_R + i\phi_I)/\sqrt{2}]^T$, $\eta = [\eta^+, (\eta_R + i\eta_I)/\sqrt{2}]^T$ and $\chi = (\chi_R + i\chi_I)/\sqrt{2}$. The mass of the SM-like Higgs h ($\equiv \phi_R$) and charged Higgs η^\pm are given by:

$$m_h^2 = \lambda_1 v^2, \quad (11)$$

$$m_{\eta^\pm}^2 = m_2^2 + \frac{1}{2}\lambda_4 v^2. \quad (12)$$

The neutral components of η and χ will mix through μ term of the potential. The mass-squared matrices spanning $(\eta_{R,I}, \chi_{R,I})$ are given by

$$\mathcal{M}_{R,I}^2 = \begin{pmatrix} m_2^2 + (\lambda_4 + \lambda_5)v^2/2 & \mu v/\sqrt{2} \\ \mu v/\sqrt{2} & m_3^2 + \lambda_6 v^2/2 \pm m_4^2 \end{pmatrix}. \quad (13)$$

Let $\zeta_{1R}, \zeta_{2R}, \zeta_{1I}, \zeta_{2I}$ be the mass eigenstates with masses $m_{1R}, m_{2R}, m_{1I}, m_{2I}$:

$$\zeta_{1R} = \cos \theta_R \eta_R - \sin \theta_R \chi_R, \quad \zeta_{2R} = \sin \theta_R \eta_R + \cos \theta_R \chi_R, \quad (14)$$

$$\zeta_{1I} = \cos \theta_I \eta_I - \sin \theta_I \chi_I, \quad \zeta_{2I} = \sin \theta_I \eta_I + \cos \theta_I \chi_I, \quad (15)$$

then the neutrino mass matrix is given by

$$(\mathcal{M}_\nu)_{ij} = \sum_k \frac{h_{ik} h_{jk} M_k}{16\pi^2} \left[\frac{\cos^2 \theta_R m_{1R}^2}{m_{1R}^2 - M_k^2} \ln \frac{m_{1R}^2}{M_k^2} + \frac{\sin^2 \theta_R m_{2R}^2}{m_{2R}^2 - M_k^2} \ln \frac{m_{2R}^2}{M_k^2} \right. \\ \left. - \frac{\cos^2 \theta_I m_{1I}^2}{m_{1I}^2 - M_k^2} \ln \frac{m_{1I}^2}{M_k^2} - \frac{\sin^2 \theta_I m_{2I}^2}{m_{2I}^2 - M_k^2} \ln \frac{m_{2I}^2}{M_k^2} \right], \quad (16)$$

where M_k are the masses of N_k . Note that in the limit of $m_4^2 = 0$, $m_{1R} = m_{1I}$, $m_{2R} = m_{2I}$, and $\theta_R = \theta_I$. Hence the neutrino mass would be zero.

We assume that m_4^2 is very small, then

$$m_{1R}^2 = m_{10}^2 + s^2 m_4^2, \quad m_{1I}^2 = m_{10}^2 - s^2 m_4^2, \quad (17)$$

$$m_{2R}^2 = m_{20}^2 + c^2 m_4^2, \quad m_{2I}^2 = m_{20}^2 - c^2 m_4^2, \quad (18)$$

$$\sin \theta_R = s \left(1 + \frac{c^2 m_4^2}{m_{10}^2 - m_{20}^2} \right), \quad \sin \theta_I = s \left(1 - \frac{c^2 m_4^2}{m_{10}^2 - m_{20}^2} \right), \quad (19)$$

$$\cos \theta_R = c \left(1 - \frac{s^2 m_4^2}{m_{10}^2 - m_{20}^2} \right), \quad \cos \theta_I = c \left(1 + \frac{s^2 m_4^2}{m_{10}^2 - m_{20}^2} \right), \quad (20)$$

where $s = \sin \theta_0$ and $c = \cos \theta_0$ which diagonalize the (η^0, χ) mass-squared matrix in the absence of m_4^2 with eigenvalues m_{10}^2 and m_{20}^2 . The one-loop neutrino mass matrix is then of the form

$$(\mathcal{M}_\nu)_{ij} = \frac{s^2 c^2 m_4^2}{8\pi^2} \sum_k h_{ik} h_{jk} M_k \left[\frac{1 - 2 \ln(m_{10}^2/M_k^2)}{m_{10}^2 - M_k^2} - \frac{1 - 2 \ln(m_{20}^2/M_k^2)}{m_{20}^2 - M_k^2} \right]. \quad (21)$$

For m_{10} of order 100 GeV and m_{20}, M of order MeV, the first term is negligible. For example, let $hs = 0.2$, $s = 0.5$, $M = 3$ MeV, $m_{20} = 4$ MeV, and $m_4^2 = (128 \text{ keV})^2$, then $m_\nu = 0.1$ eV. In this scenario, N is dark matter with a mass of 3 MeV, ζ_2 has a mass of 4 MeV and interacts with $\bar{\nu}_L N_R$ with strength 0.1. This is thus a possible scenario for neutrino interacting MeV dark matter which obtains the correct relic abundance, as discussed in Section 2. Note that the ζ_2 mass splitting is small, *i.e.* 3 keV, and both ζ_{2R} and ζ_{2I} decay to νN .

If the cosmological missing-satellite problem and the too-big-to-fail problem are solved using elastic $N\nu$ scattering, then ζ_{2R} and ζ_{2I} should be both only a few keV above M , in which case Eq. (21) is not valid. Let $m_{2R}^2 = M^2(1 + \delta_R)$ and $m_{2I}^2 = M^2(1 + \delta_I)$, with $\delta_{R,I}$ of order 10^{-3} , then the radiative neutrino mass becomes $(s^2 h^2 / 32\pi^2) M(\delta_I - \delta_R)$, which is of order 0.1 eV for $hs = 0.1$ as desired.

However, for the small couplings implied by Eqs. (8) and (9), the induced neutrino mass is negligible. On the other hand, only N_1 needs to be light, whereas $N_{2,3}$ can be heavy and the usual acceptable neutrino masses are obtained. The important point of this study (to be

justified in the subsequent sections) is that the mass of one scalar, *i.e.* ζ_2 (ζ_{2R} or ζ_{2I}), can be of order MeV. The other two neutral scalars ζ_{1R} and ζ_{1I} can be heavy. We will assume ζ_{1R} and ζ_{1I} are heavier than $m_h/2$ so that they do not contribute to the invisible Higgs width.

4 Phenomenology of the Scalar Sector: Theoretical and Experimental Constraints

The scalar potential Eq. (10) has altogether 12 parameters and 1 vacuum expectation value (vev) v . Two of them (m_1^2 and v) can be eliminated by the minimization condition and W gauge boson mass. At the LHC, both ATLAS and CMS experiments had performed several measurements of the newly discovered scalar particle in different channels. The combined measured mass performed by ATLAS and CMS collaborations based on the data from $h \rightarrow \gamma\gamma$ and $h \rightarrow ZZ \rightarrow 4l$ channels is $m_h = 125.09 \pm 0.21$ (stat.) ± 0.11 (syst.) GeV [35]. This measurement if interpreted as the SM Higgs boson allow us to fix λ_1 . We are then left with 10 independent parameters:

$$\mathcal{P} = \{\lambda_{2,3,4,5,6,7}, m_2^2, m_3^2, m_4^2, \mu\} . \quad (22)$$

In our numerical analysis presented in the next Section, these parameters are scanned in the confined domain that fulfill various theoretical and experimental constraints which are discussed below.

4.1 Theoretical Constraints

4.1.1 Unitarity Constraints

Our scalar potential is similar to the one in the 2 Higgs doublet model except augmented by a complex singlet field χ . We can carefully use the full set of unitarity constraints derived for the 2 Higgs doublet model in [36]. In Appendix A.1, we list the set of unitarity constraints

that we will use. Some of the $2 \rightarrow 2$ scattering amplitudes have been modified to take into account the presence of χ . In summary, the requirement that the largest eigenvalues of all the partial wave matrices a_0s for different channels to respect the unitarity constraints implies

$$|a_{\pm}|, |b_{\pm}|, |c_{\pm}|, |s_{1,2}|, |f_{\pm}|, |e_{1,2}|, |f_{1,2}|, |p_1| \leq 8\pi, \quad (23)$$

where the definitions of the eigenvalues (a_{\pm} , b_{\pm} , and so on in the above equation) in terms of the quartic couplings in the scalar potential can be found in Appendix A.1.

4.1.2 Vacuum Stability

A necessary condition for the stability of the vacuum comes from requiring the potential given in Eq. (10) to be bounded from below when the scalar fields become large in any direction of the field space. At large field values, the scalar potential is dominated by quartic couplings, the bounded from below constraints will depend only on the quartic couplings. The constraints ensuring tree level vacuum stability are:

- If $\lambda_6 > 0$ and $\lambda_7 > 0$,

$$\lambda_1 > 0, \quad \lambda_2 > 0, \quad \lambda_3 > 0, \quad (24)$$

$$\sqrt{\lambda_1 \lambda_2} + \lambda_4 + \lambda_5 > 0, \quad (25)$$

$$\sqrt{\lambda_1 \lambda_2} + \lambda_4 > 0. \quad (26)$$

- If $\lambda_6 < 0$ or $\lambda_7 < 0$, in addition to the above constraints, we also have

$$(\lambda_3 \lambda_1 - \lambda_6^2) > 0, \quad (27)$$

$$(\lambda_3 \lambda_2 - \lambda_7^2) > 0, \quad (28)$$

$$-\lambda_6 \lambda_7 + \lambda_3 \lambda_4 + \sqrt{(\lambda_3 \lambda_1 - \lambda_6^2)(\lambda_3 \lambda_2 - \lambda_7^2)} > 0, \quad (29)$$

$$-\lambda_6 \lambda_7 + \lambda_3(\lambda_4 + \lambda_5) + \sqrt{(\lambda_3 \lambda_1 - \lambda_6^2)(\lambda_3 \lambda_2 - \lambda_7^2)} > 0. \quad (30)$$

Additional constraints also related to the stability issue come from the requirement of the absence of tachyonic masses. They are

$$m_{\eta^+}^2 = m_2^2 + \frac{1}{2}\lambda_4 v^2 > 0 , \quad (31)$$

$$m_{1R}^2 + m_{2R}^2 = m_2^2 + m_3^2 + m_4^2 + \frac{1}{2}(\lambda_4 + \lambda_5 + \lambda_6)v^2 > 0 , \quad (32)$$

$$m_{1I}^2 + m_{2I}^2 = m_2^2 + m_3^2 - m_4^2 + \frac{1}{2}(\lambda_4 + \lambda_5 + \lambda_6)v^2 > 0 . \quad (33)$$

Details of derivation of these constraints can be found in Appendix A.2.

4.2 Experimental Constraints

4.2.1 Invisible Decay of the Higgs

Our neutrino model requires MeV warm dark matter particle which can be identified as the lightest Majorana neutrino state of $N_{1,2,3}$. The SM Higgs $h \rightarrow N_i N_i$ can occur only through one loop. Hence its branching ratio is small and we will ignore this invisible mode in our analysis. On the other hand, due to the mixing of complex field χ with the inert doublet η , we have 2 light dark Higgses ζ_{2R} and ζ_{2I} , one is CP even and one is CP odd. These states are not stable since they can decay via $\chi_D \rightarrow N\nu$ where χ_D is the lighter state of ζ_{2R} and ζ_{2I} and N is the DM, the lightest of $N_{1,2,3}$. Thus the tree level decay $h \rightarrow \chi_D \chi_D \rightarrow NN\nu\nu$ will be invisible. The SM Higgs couplings to these dark Higgses ζ_{2R} and ζ_{2I} are given in Table 1 in Appendix A.3.

The openings of one of the non-standard decays of the Higgs boson such as $h \rightarrow \zeta_i \zeta_j$ can modify the total width of the Higgs boson and can have significant impact on LHC results. Both ATLAS and CMS had performed searches for invisible decay of the Higgs boson [37, 38]. Both experiments set upper limit on the branching fraction of the invisible decays of the Higgs. These limits are of the order of 28% from ATLAS [37] or 36% from CMS [38] and will be improved further with the new LHC run at 13 and 14 TeV. This constraint on the

invisible decay is still rather weak compared to the one derived from various works of global fits to ATLAS and CMS data [39]. These global fits studies with the assumption that the Higgs boson has SM-like couplings to all SM particles plus additional invisible decay mode, suggest that the branching ratio of the invisible decay of the Higgs boson should not exceed 19% at 95% C.L. In our numerical analysis presented later, we will use this global fitting result for the invisible width of the Higgs instead of the experimental upper limits. In our model, the SM Higgs couples to all SM particles like fermions, massive gauge bosons and gluons exactly the same way as in SM. The only exceptions are $h \rightarrow \gamma\gamma$ and $h \rightarrow \gamma Z$ which receive additional contributions from charged Higgs. The Higgs total width can be modified slightly by $h \rightarrow \gamma\gamma$ and $h \rightarrow \gamma Z$ as well as by $h \rightarrow \zeta_{iR}\zeta_{jR}$ and $h \rightarrow \zeta_{iI}\zeta_{jI}$ ($i, j = 1, 2$) if these latter channels are open.

The couplings of the SM Higgs to the neutral dark Higgses $\eta_{R,I}$, $\chi_{R,I}$ is given by

$$\mathcal{F} = \begin{pmatrix} (\lambda_4 + \lambda_5)v & \mu/\sqrt{2} \\ \mu/\sqrt{2} & \lambda_6 v \end{pmatrix}. \quad (34)$$

As one can see from Eq. (13) and Eq. (34), if the matrices \mathcal{F} and $\mathcal{M}_{R,I}^2$ are proportional to each other, the Higgs couplings to ζ_{2R} and ζ_{2I} are automatically diagonal in the mass eigenstate basis and proportional to its mass squared. The conditions for \mathcal{F} and $\mathcal{M}_{R,I}^2$ to be proportional to each other, in the limit of $m_4^2 = 0$, are

$$m_2^2 = (\lambda_4 + \lambda_5)v^2/2 \quad \text{and} \quad m_3^2 = \lambda_6 v^2/2. \quad (35)$$

If these conditions are fulfilled, we have $\mathcal{M}_{R,I}^2 = v\mathcal{F}$. Once $\mathcal{M}_{R,I}^2$ are diagonalized by some orthogonal matrices, the coupling matrix \mathcal{F} will be also diagonal in the mass eigenstate basis. Therefore the couplings $h\zeta_{2R}\zeta_{2R}$ and $h\zeta_{2I}\zeta_{2I}$ will be proportional to the mass of the dark Higgses and are therefore negligible for MeV dark Higgses.

The decay rate for $h \rightarrow \zeta_a\zeta_b$ can be found in Appendix A.3. In our case only $h \rightarrow \zeta_{iR}\zeta_{jR}$ and $h \rightarrow \zeta_{iI}\zeta_{jI}$ exists. Furthermore, provided that the alignment condition of $\mathcal{M}_{R,I}^2 = v\mathcal{F}$

can be satisfied, only $h \rightarrow \zeta_{2R}\zeta_{2R}$ and $h \rightarrow \zeta_{2I}\zeta_{2I}$ will contribute to the SM Higgs invisible width. The other diagonal decays $h \rightarrow \zeta_{1R}\zeta_{1R}$ and $h \rightarrow \zeta_{1I}\zeta_{1I}$ will be kinematically not accessible if we assume $m_{\zeta_{1R}}$ and $m_{\zeta_{1I}}$ are larger than $m_h/2$.

4.2.2 Z Decay Width

The measurement of Z -boson total width Γ_Z at LEP set stringent bounds on any extra contribution $\Delta\Gamma_Z$ from new decay channels. In our case, Z can decay to $\zeta_{2R}\zeta_{2I}$ through the mixing of the neutral component of inert doublet with the complex singlet.

The $Z\zeta_a\zeta_b$ couplings are listed in Table 1 in Appendix A.3 and the corresponding tree-level decay width for each channel is given by Eq. (95) in Appendix A.4. We will only consider the decay mode $Z \rightarrow \zeta_{2R}\zeta_{2I}$ since other modes are presumably kinematically forbidden. Ignoring the masses in the final state, we have

$$\Gamma_{Z \rightarrow \zeta_{2R}\zeta_{2I}} \approx \frac{\sin^2 \theta_R \sin^2 \theta_I \sqrt{2} G_F m_Z^3}{48\pi}. \quad (36)$$

From the quoted LEP value $\Gamma_Z = 2.4952 \pm 0.0023$ GeV and the SM prediction $\Gamma_Z^{\text{SM}} = 2.4961 \pm 0.0010$ GeV [40], one can estimate the maximum allowed non-standard contribution to $\Delta\Gamma_Z^{\text{max}}$ is about 4.2 MeV at 95% C.L. Requiring that $\Gamma_{Z \rightarrow \zeta_{2R}\zeta_{2I}} \leq 4.2$ MeV, one can set the following limits on the mixing angle:

$$\sin \theta_R \sin \theta_I \leq 0.23, \quad (37)$$

$$\sin \theta_R \approx \sin \theta_I \leq 0.47. \quad (38)$$

4.2.3 S and T Parameters

If the scale of new physics is much larger than the electroweak scale, virtual effect of the new particles in the loops are expected to contribute through vacuum polarization corrections to the electroweak precision observables. These corrections are known as oblique corrections

and are parameterized by S , T and U parameters [41]. In our case, the inert Higgs doublet couples to the W and Z gauge bosons via the covariant derivative. Due to mixing effects, the complex singlet χ will couple to the weak gauge bosons as well. Therefore, both η and χ will contribute to S and T parameters which are very well constrained by electroweak precision data. Analytic formulas for ΔS and ΔT modified by the mixing angles as compared with the IHDM formulas are collected in Appendix A.5 for convenience. Thus our model will remain viable as long as ΔS and ΔT are compatible with the fitted values [42] which are given by:

$$\Delta S = 0.06 \pm 0.09 \quad \text{and} \quad \Delta T = 0.10 \pm 0.07 . \quad (39)$$

4.2.4 LEP Limits

Due to the Z_2 symmetry, all interactions that involve the dark Higgses must contain a pair of them. The precise measurements of W and Z widths at LEP [40] can be used to set a limit on the mass of the inert Higgses. In order not to significantly modify the decay widths of W and Z , we request that the channels $W^\pm \rightarrow \{\zeta_{iR}\eta^\pm, \zeta_{iI}\eta^\pm\}$ and/or $Z \rightarrow \{\zeta_{iR}\zeta_{jI}, \eta^+\eta^-\}$ are kinematically closed. This leads to the following constraints:

$$m_{\zeta_{iI}} + m_{\eta^\pm} > m_W \quad , \quad m_{\zeta_{iR}} + m_{\eta^\pm} > m_W \quad (40)$$

$$m_{\zeta_{iR}} + m_{\zeta_{jI}} > m_Z \quad , \quad m_{\eta^\pm} > m_Z/2 \quad , \quad i, j = 1, 2 \quad (41)$$

At e^+e^- colliders, the production mechanism for inert Higgs is

$$e^+e^- \rightarrow \eta^\pm\eta^\mp \quad , \quad e^+e^- \rightarrow \zeta_{iR}\zeta_{jI} \quad , \quad (42)$$

while at hadron machines we have

$$q\bar{q} \rightarrow \eta^\pm\eta^\mp \quad , \quad q\bar{q} \rightarrow \zeta_{iR}\zeta_{jI} \quad , \quad (43)$$

$$q'\bar{q} \rightarrow \eta^\pm\zeta_{iR} \quad , \quad q'\bar{q} \rightarrow \eta^\pm\zeta_{iI} \quad . \quad (44)$$

Because of Z_2 , the inert Higgs can not decay to SM fermions. Thus the LEP II and Tevatron searches for charged Higgs and neutral Higgs can not be applied to our model. The inert charged Higgs can decay via $\eta^\pm \rightarrow W^\pm \zeta_{2R}, W^\pm \zeta_{2I}$ or through cascade decay via $\eta^\pm \rightarrow W^\pm \zeta_{1R} \rightarrow W^\pm Z \zeta_{2I}$ or $\eta^\pm \rightarrow W^\pm \zeta_{1I} \rightarrow W^\pm Z \zeta_{2R}$. Similarly, the neutral dark Higgses ζ_{1R} and ζ_{1I} can decay into $Z \zeta_{2I}$ and $Z \zeta_{2R}$ respectively, or through cascade decays like $\zeta_{1R} \rightarrow \eta^\pm W^\mp \rightarrow W^\pm W^\mp \zeta_{2I}$ and $\zeta_{1I} \rightarrow \eta^\pm W^\mp \rightarrow W^\pm W^\mp \zeta_{2R}$. In all cases the final states of these production mechanisms both at lepton or hadron colliders would be multi-leptons or multi-jets, depending on the decay products of W^\pm and Z , plus missing energies carried by the dark Higgses.

To certain extent, the signatures for the inert charged or neutral Higgses would be similar to the supersymmetry searches for charginos and neutralinos at the e^+e^- or hadron colliders. Detailed phenomenological implications of this model at the LHC are interesting to explore but it is beyond the scope of this present work.

4.2.5 Constraints from LHC

Both ATLAS and CMS experiments of the LHC run at $7 \oplus 8$ TeV confirmed the discovery of a scalar particle with mass around 125 GeV identified to be the Higgs field h in our model. Both groups performed several measurements on this scalar particle couplings to the SM particles such as W^+W^- , ZZ , $\gamma\gamma$ and $\tau^+\tau^-$ with 20 – 30% uncertainties, while for $b\bar{b}$ it suffers from larger uncertainty of 40 – 50%. Recently ATLAS [43] published an updated analysis of $7 \oplus 8$ TeV data in which the signal strengths $2.7^{+4.6}_{-4.5}$ for $h \rightarrow \gamma Z$ and $-0.7^{+3.7}_{-3.7}$ for $h \rightarrow \mu^+\mu^-$ were reported. Basically, all the LHC data collected so far indicates that the 125 GeV boson couplings to the SM particles are very much SM-like. One of the main tasks of the new LHC run at 13 TeV would be to improve all the aforementioned measurements and probe for new ones, such as $h \rightarrow \gamma Z$, $\mu^+\mu^-$ and perhaps the trilinear self-coupling of

the Higgs. It is expected that the new run of LHC will narrow down the uncertainties of $hb\bar{b}$ and $h\tau^+\tau^-$ measurements to $10 - 13\%$ and $6 - 8\%$ respectively. In the future, if the high luminosity option for LHC (HL-LHC) is available, it can do much to ameliorate the uncertainties to $4 - 7\%$ ($hb\bar{b}$) and $2 - 5\%$ ($h\tau^+\tau^-$) [44]; while for the e^+e^- Linear Collider (LC), these uncertainties can be cut down further to 0.6% ($hb\bar{b}$) and 1.3% ($h\tau^+\tau^-$) [44, 45].

While the tree level SM Higgs couplings to fermions and to weak gauge bosons in our model are identical to the SM one, the loop mediated processes such as $h \rightarrow \gamma\gamma$ and $h \rightarrow \gamma Z$ will receive additional contributions from inert charged Higgs loop that can either enhance or suppress their partial widths [46]. On the other hand, the invisible decay of the SM Higgs into dark Higgs pair is very much suppressed in our model. As a consequence the total width of the SM Higgs will be modified slightly through the additional charged Higgs contributions in the $h \rightarrow \gamma\gamma$ and $h \rightarrow \gamma Z$ modes. ATLAS and CMS collaborations usually present their results in terms of the so-called signal strengths. For a given production channel and a given decay mode of the SM Higgs, the signal strength is defined as

$$R_{YZ} \equiv \frac{\sigma(h + X) \times \text{Br}(h \rightarrow YZ)}{\sigma^{\text{SM}}(h + X) \times \text{Br}^{\text{SM}}(h \rightarrow YZ)} , \quad (45)$$

where the Higgs mass is evaluated to be the same in both numerator and denominator.

In our analysis for the signal strengths, we will use the following ATLAS results [43]:

- $h \rightarrow \gamma\gamma$: $R_{\gamma\gamma} = 1.17 \pm 0.27$
- $h \rightarrow ZZ$: $R_{ZZ} = 1.44^{+0.40}_{-0.33}$
- $h \rightarrow W^+W^-$: $R_{WW} = 1.16^{+0.24}_{-0.21}$
- $h \rightarrow \tau^+\tau^-$: $R_{\tau^+\tau^-} = 1.43^{+0.43}_{-0.37}$

5 Numerical Results

We now present our numerical results with the implementation of all the theoretical and experimental constraints on the parameter space discussed in the previous Section. Let us classify the dimensionless parameters λ_i in the scalar potential into two different sets according to the following two types of constraints:

- First set of constraints includes the unitarity constraints in Eq. (23), vacuum stability constraints in Eqs. (24)-(27) and also non-tachyonic masses in Eqs. (31)-(33). We refer this set of constraints as C_1 .
- The second set of constraints contains the invisible decay of the Z boson in Eq. (38), ΔS and ΔT constraints in Eq. (39), signal strength constraints on $R_{\gamma\gamma}$, R_{WW} , R_{ZZ} and $R_{\tau^+\tau^-}$ listed in the end of Section (4.2.5). We also require the masses of ζ_{1R} , ζ_{1I} and η^\pm to be heavier than 100 GeV. We refer this set of constraints as C_2 .

Since λ_1 is fixed by the SM Higgs mass, we scan over the other $\lambda_i \in \mathcal{P}$ in the following range

$$0 < \lambda_{2,3} \leq 4\pi , \quad (46)$$

$$|\lambda_{4,5,6,7}| \leq 4\pi . \quad (47)$$

For the dimensional mass parameters in the scalar potential, m_1^2 is fixed by the SM Higgs mass, and m_2^2 and m_3^2 are fixed by Eq. (35) in order to suppress the invisible decay of the SM Higgs. For the m_4^2 and μ parameters, they will be chosen in such a way to allow for MeV dark Higgses ζ_{2R} and ζ_{2I} . Recall that their masses are provided by the smaller eigenvalues of the two mass matrices in Eq. (13),

$$m_{\zeta_{2R}, \zeta_{2I}}^2 = \frac{1}{2} \left(A + C - \sqrt{(A - C)^2 + 4B^2} \right) , \quad (48)$$

where A , B and C are given by ²

$$A = m_2^2 + \frac{1}{2}(\lambda_4 + \lambda_5)v^2, \quad (49)$$

$$B = \frac{1}{\sqrt{2}}\mu v, \quad (50)$$

$$C = m_3^2 + \frac{1}{2}\lambda_6 v^2 \pm m_4^2. \quad (51)$$

To obtain very light dark Higgses, we fine tune $A + C$ and $\sqrt{(A - C)^2 + 4B^2}$ to be almost the same size. Define

$$\epsilon \equiv \frac{1}{2}(A + C - \sqrt{(A - C)^2 + 4B^2}). \quad (52)$$

Assuming ϵ is small and dropping the ϵ^2 term, we have

$$B^2 = \mu^2 v^2 / 2 \sim AC - \epsilon(A + C). \quad (53)$$

For given ϵ , A and C , the μ parameter is determined. If we further drop the ϵ term in Eq. (53), it would give an additional constraint on the sign of the product $AC > 0$:

$$AC = (m_2^2 + (\lambda_4 + \lambda_5)v^2/2)(m_3^2 + \lambda_6 v^2/2) = (\lambda_4 + \lambda_5)(\lambda_6)v^4 > 0, \quad (54)$$

where Eq. (35) has been applied in the last equality. Thus $\lambda_4 + \lambda_5$ and λ_6 should have the same sign. On the other hand, neglecting m_4^2 in C , Eqs. (35), (49) and (51) imply

$$A + C = (\lambda_4 + \lambda_5 + \lambda_6)v^2 > 0. \quad (55)$$

Combining Eqs. (54) and (55), one can conclude $\lambda_4 + \lambda_5$ and λ_6 should be positive, at least for small ϵ and m_4^2 . Numerically, we set $\epsilon/\text{GeV}^2 = 10^{-4}$ and $m_4^2/\text{GeV}^2 = 10^{-5}$ in our analysis.

A systematic scan on λ_i in the range defined in Eq. (47) indicated that λ_2 and λ_3 are not very much restricted by all the above constraints. In Fig. (2) we illustrate the allowed range

²For the heavier states ζ_{1R} and ζ_{1I} , their masses are given by $(A + C + \sqrt{(A - C)^2 + 4B^2})/2$.

for (λ_4, λ_5) (left panel) and for (λ_6, λ_7) (right panel). Red points pass C_1 set of constraints while green points pass both C_1 and C_2 .

We have checked that all the red points in the left panel of Fig. (2) fall in the following domain:

$$|\lambda_4 + 2\lambda_5| \leq 8\pi \quad \text{and} \quad |\lambda_4 - \lambda_5| \leq 8\pi, \quad (56)$$

which are the unitarity constraints. Imposing the vacuum stability constraints reduce further the above domain. As one can see from the plot in the left panel, imposing merely the constraint set C_1 , λ_5 could be either positive or negative while λ_4 is mostly positive except for a small negative range of $[-1.3, 0]$. This small negative range for λ_4 is further reduced when we apply the C_2 constraint set. Later we will see that the sign of λ_4 is important for charged Higgs contribution to $h \rightarrow \gamma\gamma$.

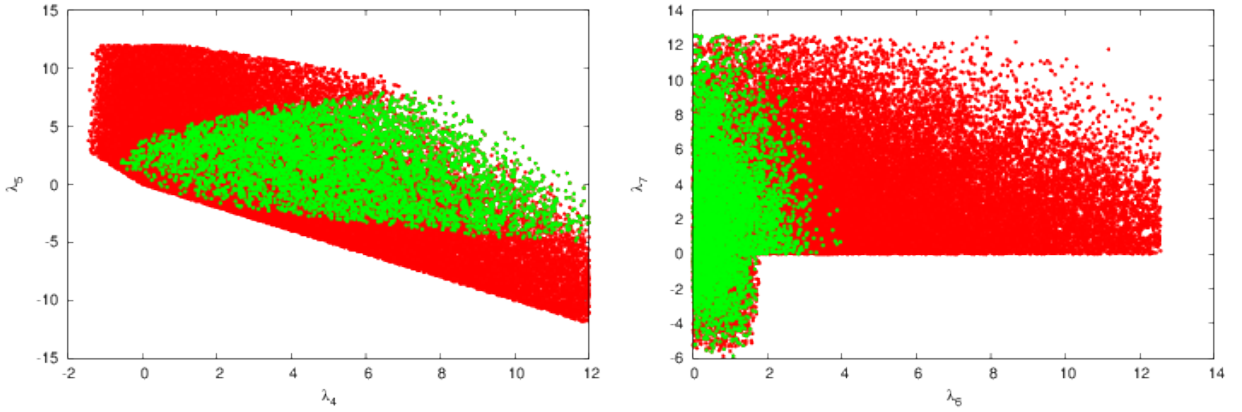


Figure 2: Allowed range for (λ_4, λ_5) (left) and (λ_6, λ_7) (right). Red points pass C_1 set, green points pass both C_1 and C_2 sets.

From our previous discussion we demonstrated that under our assumptions λ_6 is positive. It is clear from the plot at the right panel of Fig. (2) that when λ_6 and λ_7 are both positive, the C_1 constraint set does not restrain λ_6 and λ_7 too much. Even when both C_1 and C_2 are imposed, λ_7 is not very much constrained while the range of λ_6 has shrunk significantly.

This is due to the fact that λ_7 does not contribute to the masses of dark Higgses while λ_6 does.

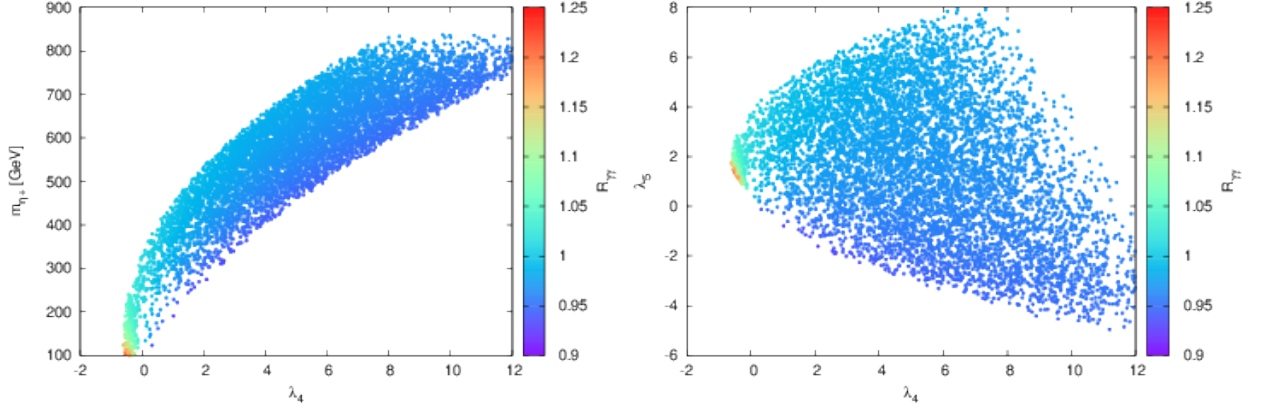


Figure 3: Scatter plot for $R_{\gamma\gamma}$ in $(\lambda_4, m_{\eta^\pm})$ plane (left) and in (λ_4, λ_5) plane (right). All points pass both C_1 and C_2 sets.

In the left and right panels of Fig. (3) we present the scatter plots of the signal strength $R_{\gamma\gamma}$, represented by the color palettes located at the right sides of both panels, on the $(\lambda_4, m_{\eta^\pm})$ and (λ_4, λ_5) planes respectively. In these two plots, both C_1 and C_2 constraint sets are imposed. In our model, since the SM Higgs is produced exactly the same way as in the SM, the production cross sections in the numerator and denominator of $R_{\gamma\gamma}$ cancel, and the signal strength is simply given by the ratio of branching fractions. Thus $R_{\gamma\gamma}$ is independent of the LHC energy at Run 1 or 2.

As is well known the loop contributions in $h \rightarrow \gamma\gamma$ is fully dominated by W^\pm with some subleading contribution from top quark which interferes destructively with the W^\pm . As alluded earlier, $h \rightarrow \gamma\gamma$ receives additional contribution from charged Higgs η^\pm in this model [46]. The coupling of the SM Higgs to the η^\pm pair is proportional to λ_4 . If λ_4 is negative (positive) then the η^\pm loop is constructively (destructively) interference with the W^\pm s, resulting in an enhanced (suppressed) $h \rightarrow \gamma\gamma$ rate with respect to SM one. By comparing with the color palettes for $R_{\gamma\gamma}$ on the right side of both panels of Fig. (3), it is

evident that $R_{\gamma\gamma}$ is enhanced for negative λ_4 but suppressed for positive λ_4 . Note that λ_4 is restricted only to a small range of negative λ_4 $[-0.65, 0]$ which could enhance $h \rightarrow \gamma\gamma$ rate with respect to SM. This range of negative λ_4 corresponds to λ_5 in the range $[0.5, 3.7]$. These two ranges for λ_4 and λ_5 imply that the charged Higgs η^\pm is in $[100, 325]$ GeV range where $R_{\gamma\gamma} > 1$. It is clear from the left panel of Fig. (3) that larger η^\pm mass (and so as the two other neutral dark Higgses $\zeta_{1R,1I}$) say 500 GeV is also possible. But then the signal strength of $R_{\gamma\gamma}$ would be very close to its SM value.

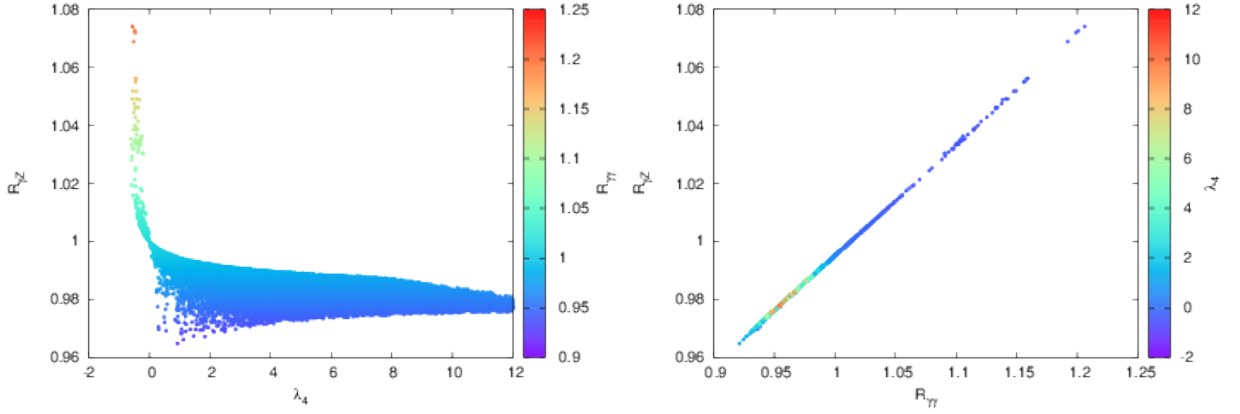


Figure 4: (Left) $R_{\gamma Z}$ as a function of λ_4 with $R_{\gamma\gamma}$ shown in palette at the right. (Right) Correlation between $R_{\gamma Z}$ and $R_{\gamma\gamma}$ with λ_4 shown in palette at the right.

In Fig. (4) we illustrate $R_{\gamma Z}$ and its correlation with $R_{\gamma\gamma}$. In the left panel, we show $R_{\gamma Z}$ as a function of λ_4 while scanning all other parameters. As in the $R_{\gamma\gamma}$ case, $R_{\gamma Z}$ is enhanced for negative λ_4 but suppressed for positive λ_4 with respect to SM. In the right panel we show the correlation between $R_{\gamma\gamma}$ and $R_{\gamma Z}$. At the point $\lambda_4 = 0$, the charged Higgs contribution vanishes and both $R_{\gamma\gamma}$ and $R_{\gamma Z}$ reduces to their SM values. It is interesting to note that for $R_{\gamma\gamma} > 1$ we have $1 < R_{\gamma Z} < R_{\gamma\gamma}$ while for $R_{\gamma\gamma} < 1$ we have $R_{\gamma Z} > R_{\gamma\gamma}$. These predictions can be tested at LHC Run II.

6 Conclusion

In this work, we have presented a realistic renormalizable model with one-loop induced neutrino mass via the interactions of neutrinos with MeV dark matter. Besides the SM doublet, one extra scalar doublet and one complex singlet were introduced in the scalar sector. Moreover, three light singlet Majorana fermions were needed for the one-loop mechanism producing the neutrino masses. All these new fields transform under a global dark $U(1)_D$ symmetry, which is broken softly into Z_2 by a single term in the scalar potential as well as by the assumed Majorana masses of the new fermion singlets. The lightest of these Majorana fermions is the MeV warm dark matter while some of the new scalars mixed and can give rise to two MeV dark Higgses. Besides the 125 GeV SM Higgs, other heavier scalars include one charged Higgs and two neutral dark Higgses, which can have masses of several hundreds GeV.

In order to suppress the decay of the SM Higgs into pair of dark Higgses we require its coupling matrix with the dark Higgses aligns with the mass matrix of the dark Higgses. For light dark Higgs masses, the invisible branching ratio of the SM Higgs into dark Higgses will then be suppressed and easily satisfies the global fit results as well as the LHC limits of the SM Higgs invisible width.

We have studied the theoretical as well as experimental constraints imposed on the scalar sector of the model in some detail. We have pinned down the parameter space of the model consistent with these constraints. Our numerical results indicate that the proposed model is realistic. It is possible to accommodate both sub-eV neutrino masses and MeV dark matter in a renormalizable model with a global dark $U(1)_D$ symmetry softly breaking into Z_2 . Some additional scalar particles of electroweak scale can be obtained. Further collider implications of the model may be worthy of further investigation.

Acknowledgment : AA and TCY would like to thank the hospitality of Physics Division of NCTS Taiwan where this work was made progress. This work is supported by the U. S. Department of Energy under Grant No. DE-SC0008541 (EM), the Ministry of Science and Technology of Taiwan under grant number 104-2112-M-001-001-MY3 (TCY) and the Moroccan Ministry of Higher Education and Scientific Research MESRSFC and CNRST: “Projet dans les domaines prioritaires de la recherche scientifique et du d’eveloppement technologique”: PPR/2015/6 (AA).

Appendix A

A.1 Perturbative Unitarity Constraints

To constrain the scalar potential parameters, one can demand that tree-level unitarity is preserved in a variety of $2 \rightarrow 2$ scattering processes.

Since our model is a 2 Higgs doublet extended with a singlet field, we can use the same procedure developed in [36] to derive the unitarity constraints. According to [36], one computes the S matrix in the non-physical fields basis where the computation is much easier. The crucial point is that the S matrix expressed in terms of the physical fields (*i.e.* the mass eigenstate fields) can be transformed into an S matrix for the non-physical fields by making a unitary transformation. The eigenvalues for the S matrix should be unchanged under such a unitary transformation.

The first submatrix \mathcal{M}_1 , corresponding to scatterings whose initial and final states being

one of the following combinations $(w_1^+ w_2^-, w_2^+ w_1^-, \phi_R \eta_I, \eta_R \phi_I, \phi_I \eta_I, \phi_R \eta_R)$, is given by

$$\mathcal{M}_1 = \begin{pmatrix} \lambda_4 + \lambda_5 & 0 & -\frac{\lambda_5}{2} & \frac{\lambda_5}{2} & \frac{\lambda_5}{2} & \frac{\lambda_5}{2} \\ 0 & \lambda_4 + \lambda_5 & \frac{\lambda_5}{2} & -\frac{\lambda_5}{2} & \frac{\lambda_5}{2} & \frac{\lambda_5}{2} \\ \frac{\lambda_5}{2} & -\frac{\lambda_5}{2} & \lambda_4 + \lambda_5 & 0 & 0 & 0 \\ -\frac{\lambda_5}{2} & \frac{\lambda_5}{2} & 0 & \lambda_4 + \lambda_5 & 0 & 0 \\ \frac{\lambda_5}{2} & \frac{\lambda_5}{2} & 0 & 0 & \lambda_4 + \lambda_5 & 0 \\ \frac{\lambda_5}{2} & \frac{\lambda_5}{2} & 0 & 0 & 0 & \lambda_4 + \lambda_5 \end{pmatrix}. \quad (57)$$

Its eigenvalues are determined as

$$e_1 = \lambda_4 + 2\lambda_5, \quad (58)$$

$$e_2 = \lambda_4, \quad (59)$$

$$f_+ = \lambda_4 + 2\lambda_5, \quad (60)$$

$$f_- = e_2, \quad (61)$$

$$f_1 = f_2 = \lambda_4 + \lambda_5. \quad (62)$$

The second submatrix \mathcal{M}_2 corresponds to scattering with initial and final states belonged to one of the following states $(w_1^+ w_1^-, w_2^+ w_2^-, \frac{\phi_I \phi_I}{\sqrt{2}}, \frac{\eta_I \eta_I}{\sqrt{2}}, \frac{\phi_R \phi_R}{\sqrt{2}}, \frac{\eta_R \eta_R}{\sqrt{2}}, \frac{\chi_R \chi_R}{\sqrt{2}}, \frac{\chi_I \chi_I}{\sqrt{2}})$, where the $\sqrt{2}$ accounts for identical particle statistics. This matrix mixes doublet with singlet states and is given by

$$\mathcal{M}_2 = \begin{pmatrix} 2\lambda_1 & \lambda_{45} & \frac{\lambda_1}{\sqrt{2}} & \frac{\lambda_1}{\sqrt{2}} & \frac{\lambda_4}{\sqrt{2}} & \frac{\lambda_4}{\sqrt{2}} & \frac{\lambda_6}{\sqrt{2}} & \frac{\lambda_6}{\sqrt{2}} \\ \lambda_{45} & 2\lambda_2 & \frac{\lambda_4}{\sqrt{2}} & \frac{\lambda_4}{\sqrt{2}} & \frac{\lambda_2}{\sqrt{2}} & \frac{\lambda_2}{\sqrt{2}} & \frac{\lambda_7}{\sqrt{2}} & \frac{\lambda_7}{\sqrt{2}} \\ \frac{\lambda_1}{\sqrt{2}} & \frac{\lambda_4}{\sqrt{2}} & \frac{3\lambda_1}{2} & \frac{\lambda_1}{2} & \frac{\lambda_{45}}{2} & \frac{\lambda_{45}}{2} & \frac{\lambda_6}{2} & \frac{\lambda_6}{2} \\ \frac{\lambda_1}{\sqrt{2}} & \frac{\lambda_4}{\sqrt{2}} & \frac{\lambda_1}{2} & \frac{3\lambda_1}{2} & \frac{\lambda_{45}}{2} & \frac{\lambda_{45}}{2} & \frac{\lambda_6}{2} & \frac{\lambda_6}{2} \\ \frac{\lambda_4}{\sqrt{2}} & \frac{\lambda_2}{\sqrt{2}} & \frac{\lambda_{45}}{2} & \frac{\lambda_{45}}{2} & \frac{3\lambda_2}{2} & \frac{\lambda_2}{2} & \frac{\lambda_7}{2} & \frac{\lambda_7}{2} \\ \frac{\lambda_4}{\sqrt{2}} & \frac{\lambda_2}{\sqrt{2}} & \frac{\lambda_{45}}{2} & \frac{\lambda_{45}}{2} & \frac{\lambda_2}{2} & \frac{3\lambda_2}{2} & \frac{\lambda_7}{2} & \frac{\lambda_7}{2} \\ \frac{\lambda_6}{\sqrt{2}} & \frac{\lambda_7}{\sqrt{2}} & \frac{\lambda_6}{2} & \frac{\lambda_6}{2} & \frac{\lambda_7}{2} & \frac{\lambda_7}{2} & \frac{3\lambda_3}{2} & \frac{\lambda_3}{2} \\ \frac{\lambda_6}{\sqrt{2}} & \frac{\lambda_7}{\sqrt{2}} & \frac{\lambda_6}{2} & \frac{\lambda_6}{2} & \frac{\lambda_7}{2} & \frac{\lambda_7}{2} & \frac{\lambda_3}{2} & \frac{3\lambda_3}{2} \end{pmatrix}, \quad (63)$$

where $\lambda_{45} = \lambda_4 + \lambda_5$. This matrix has 8 eigenvalues. Five of them are

$$c_+ = \lambda_1 , \quad (64)$$

$$c_- = \lambda_2 , \quad (65)$$

$$s_1 = \lambda_3 , \quad (66)$$

$$a_{\pm} = \frac{1}{2}(\lambda_1 + \lambda_2 \pm \sqrt{(\lambda_1 - \lambda_2)^2 + 4\lambda_5^2}) . \quad (67)$$

The other 3 eigenvalues b_{\pm} and s_2 are solutions of the following polynomial

$$\begin{aligned} P(X) = & 2[3\lambda_2\lambda_6^2 + (2\lambda_4 + \lambda_5)(2\lambda_4\lambda_3 + \lambda_5\lambda_3 - 2\lambda_6\lambda_7) + 3\lambda_1(-3\lambda_2\lambda_3 + \lambda_7^2)] - \\ & [-9\lambda_1\lambda_2 + (2\lambda_4 + \lambda_5)^2 - 6\lambda_{12}\lambda_3 + 2(\lambda_6^2 + \lambda_7^2)]X - [3\lambda_{12} + 2\lambda_3]X^2 + X^3 \end{aligned} \quad (68)$$

where $\lambda_{12} = \lambda_1 + \lambda_2$.

The third submatrix \mathcal{M}_3 expressed in the basis $(\phi_R\phi_I, \eta_R\eta_I)$ is diagonal with $c_{\pm} = \lambda_{1,2}$ as eigenvalues as defined previously.

With the two singlet components, more states such as $(\phi_R\chi_I, \eta_R\chi_I)$, $(\phi_R\chi_R, \eta_R\chi_R)$, $(\phi_R\chi_{R,I}, \phi_I\chi_{R,I})$, $(\eta_R\chi_{R,I}, \eta_I\chi_{R,I})$, *etc.* can be constructed. But their corresponding scattering matrices will be diagonal and lead to either λ_6 or λ_7 as eigenvalues. These scattering states will not lead to any nontrivial constraints among λ_i since they are required to be perturbative, namely $|\lambda_i| \leq 4\pi$ for all i .

In our analysis we also include the following two body scattering processes among the 8 charged states $(\phi_R w_1^+, \eta_R w_1^+, \phi_I w_1^+, \eta_I w_1^+, \phi_R \eta^+, \eta_R \eta^+, \phi_I \eta^+, \eta_I \eta^+)$. This submatrix only lead to one additional constraint which is

$$p_1 = \lambda_4 - \lambda_5 . \quad (69)$$

The others are duplicated with the previous cases.

With the two singlet components, we can also construct charged states like $(\chi_R w_1^+, \chi_I w_1^+)$ and $(\chi_R \eta^+, \chi_I \eta^+)$ which decouple from the previous charged scattering processes. Again, the scattering matrices in these cases are diagonal with eigenvalues λ_6 and λ_7 respectively.

All the eigenvalues shown in this appendix are required to satisfy the perturbative unitarity constraints as given by Eq. (23).

A.2 Vacuum Stability Constraints on Scalar Potential

At large field values the potential Eq. (10) is dominated only by the part containing the terms that are quartic in the fields

$$\begin{aligned} V_{\text{quartic}} &= \frac{1}{2}\lambda_1(\Phi^\dagger\Phi)^2 + \frac{1}{2}\lambda_2(\eta^\dagger\eta)^2 + \lambda_4(\eta^\dagger\eta)(\Phi^\dagger\Phi) + \lambda_5(\eta^\dagger\Phi)(\Phi^\dagger\eta) \\ &+ \frac{1}{2}\lambda_3(\chi^*\chi)^2 + \lambda_6(\chi^*\chi)(\Phi^\dagger\Phi) + \lambda_7(\chi^*\chi)(\eta^\dagger\eta) . \end{aligned} \quad (70)$$

The study of V_{quartic} will thus be sufficient to obtain the main constraints from vacuum stability considerations.

Following [47], we adopt the following parameterization of the fields. First, we introduce the unit spinors $\hat{\Phi}$ and $\hat{\eta}$ such that

$$\begin{aligned} \Phi &= |\Phi|\hat{\Phi} \quad , \quad \eta = |\eta|\hat{\eta} \quad , \quad \Phi^\dagger\Phi = |\Phi|^2 \quad , \quad \eta^\dagger\eta = |\eta|^2 \\ \Phi^\dagger\eta &= |\eta||\Phi|(\hat{\Phi}^\dagger \cdot \hat{\eta}) . \end{aligned} \quad (71)$$

$(\hat{\Phi}^\dagger \cdot \hat{\eta})$ is a scalar product of 2 unit spinors which can be written as $a + ib = \rho e^{i\gamma}$ ($\rho = |a + ib| \in [0, 1]$). We then have the following parameterization

$$|\Phi| = r \cos \theta \sin \phi , \quad (72)$$

$$|\eta| = r \sin \theta \sin \phi , \quad (73)$$

$$\Phi^\dagger\eta = |\Phi||\eta|\rho e^{i\gamma} = r^2 \cos \theta \sin \theta \sin^2 \phi , \quad (74)$$

$$|\chi| = r \cos \phi , \quad (75)$$

when Φ , η and χ scan all the field space, r scans the domain $[0, \infty)$, $\rho \in [0, 1]$, and the angles $\theta, \phi \in [0, \pi/2]$. The phase γ will not have any effect here. Our potential does not have $(\Phi^\dagger \eta)^2$ as a quartic term in the potential because of dark $U(1)_D$ invariance.

One can rewrite the quartic terms using the new parameterization as

$$V_{\text{quartic}} = r^4 \left\{ \left[\frac{\lambda_1}{2} \cos^4 \theta + \frac{\lambda_2}{2} \sin^4 \theta + (\lambda_4 + \lambda_5 \rho^2) \sin^2 \theta \cos^2 \theta \right] \sin^4 \phi + \frac{\lambda_3}{2} \cos^4 \phi + [\lambda_6 \cos^2 \theta + \lambda_7 \sin^2 \theta] \cos^2 \phi \sin^2 \phi \right\}, \quad (76)$$

$$= r^4 \left\{ \left(\frac{\lambda_1}{2} \cos^4 \theta + \frac{\lambda_2}{2} \sin^4 \theta + (\lambda_4 + \lambda_5 \rho^2) \sin^2 \theta \cos^2 \theta \right) x^2 + \frac{\lambda_3}{2} (1-x)^2 + (\lambda_6 \cos^2 \theta + \lambda_7 \sin^2 \theta) x(1-x) \right\}, \quad (77)$$

where we have used $x = \sin \phi$. In this form, V_{quartic}/r^4 is a second degree polynomial in $x \in [0, 1]$. One can show that V_{quartic}/r^4 is positive if and only if ³

$$\mathcal{A} \equiv \frac{\lambda_1}{2} y^2 + \frac{\lambda_2}{2} (1-y)^2 + (\lambda_4 + \lambda_5 \rho^2) y(1-y) > 0, \quad (78)$$

$$\mathcal{B} \equiv \frac{1}{2} \lambda_3 > 0, \quad (79)$$

$$\mathcal{C} \equiv (\lambda_6 y + \lambda_7 (1-y)) > -2\sqrt{\mathcal{A}\mathcal{B}}, \quad (80)$$

where we used $y = \cos^2 \theta$. The first condition (Eq. (78)) is nothing but a scalar potential without the singlet field. This condition will give us the boundedness from below for 2 Higgs doublet model. We note that \mathcal{A} is a second degree polynomial in y . It is positive, if and only if

$$\lambda_1 > 0, \quad \lambda_2 > 0, \quad (81)$$

$$\lambda_4 + \lambda_5 \rho^2 > -\sqrt{\lambda_1 \lambda_2}, \quad \rho \in [0, 1]. \quad (82)$$

The last condition of the above equation gives the following 2 conditions

$$\lambda_4 + \sqrt{\lambda_1 \lambda_2} > 0 \quad \text{and} \quad \lambda_4 + \lambda_5 + \sqrt{\lambda_1 \lambda_2} > 0. \quad (83)$$

³ $ax^2 + b(1-x)^2 + cx(1-x) = (\sqrt{a}x - \sqrt{b}(1-x))^2 + (c + 2\sqrt{ab})x(1-x)$ is positive if and only if $a > 0$, $b > 0$ and $c > -2\sqrt{ab}$.

With the presence of the singlet field, we have from Eqs. (79) and (80)

- $\lambda_3 > 0$ from $\mathcal{B} > 0$.
- If $\lambda_6 > 0$ and $\lambda_7 > 0$, since $y \in [0, 1]$ the third constraint $\lambda_6 y + \lambda_7(1 - y) > -2\sqrt{\mathcal{A}\mathcal{B}}$ is satisfied for any $\lambda_6 > 0$ and $\lambda_7 > 0$. In this case they will be no additional constraints on $\lambda_6 > 0$ and $\lambda_7 > 0$.
- If $\lambda_6 < 0$ or $\lambda_7 < 0$, one has $-2\sqrt{\mathcal{A}\mathcal{B}} < \lambda_6 y + \lambda_7(1 - y) < 2\sqrt{\mathcal{A}\mathcal{B}}$. If not, $\lambda_6 y + \lambda_7(1 - y) > 2\sqrt{\mathcal{A}\mathcal{B}}$ will lead to $\lambda_{6,7} > 0$ which is not the case.

Then we can rewrite the third condition $\mathcal{C} > -2\sqrt{\mathcal{A}\mathcal{B}}$ (Eq. (80)) as

$$(\lambda_3\lambda_1 - \lambda_6^2)y^2 + (\lambda_3\lambda_2 - \lambda_7^2)(1 - y)^2 + (-2\lambda_6\lambda_7 + 2\lambda_3(\lambda_4 + \lambda_5\rho^2))y(1 - y) > 0, \quad (84)$$

which is positive, if and only if

$$(\lambda_3\lambda_1 - \lambda_6^2) > 0, \quad (85)$$

$$(\lambda_3\lambda_2 - \lambda_7^2) > 0, \quad (86)$$

$$(-2\lambda_6\lambda_7 + 2\lambda_3(\lambda_4 + \lambda_5\rho^2)) > -\sqrt{4(\lambda_3\lambda_1 - \lambda_6^2)(\lambda_3\lambda_2 - \lambda_7^2)}. \quad (87)$$

The 2 constraints of Eqs. (85) and (86) will give

$$\sqrt{\lambda_3\lambda_1} + \lambda_6 > 0 \quad \text{and} \quad \sqrt{\lambda_3\lambda_1} - \lambda_6 > 0, \quad (88)$$

$$\sqrt{\lambda_3\lambda_2} + \lambda_7 > 0 \quad \text{and} \quad \sqrt{\lambda_3\lambda_2} - \lambda_7 > 0. \quad (89)$$

If we work out the third condition of Eq. (87), we get

$$-\lambda_6\lambda_7 + \lambda_3\lambda_4 > -\sqrt{(\lambda_3\lambda_1 - \lambda_6^2)(\lambda_3\lambda_2 - \lambda_7^2)}, \quad (90)$$

$$-\lambda_6\lambda_7 + \lambda_3(\lambda_4 + \lambda_5) > -\sqrt{(\lambda_3\lambda_1 - \lambda_6^2)(\lambda_3\lambda_2 - \lambda_7^2)}. \quad (91)$$

In our analysis, we impose all the constraints derived in this appendix for the quartic couplings λ_i .

A.3 Scalar Cubic Couplings of the SM Higgs

Table 1: General coupling coefficients of $h\zeta_a\zeta_b$ and $Z\zeta_a\zeta_b$ vertices.

(a, b)	g_{ab}	c_{ab}
$(1R, 1R)$	$((\lambda_4 + \lambda_5) \cos^2 \theta_R + \lambda_6 \sin^2 \theta_R) - \frac{\sqrt{2}}{2} \frac{\mu}{v} \sin 2\theta_R$	0
$(2R, 2R)$	$((\lambda_4 + \lambda_5) \sin^2 \theta_R + \lambda_6 \cos^2 \theta_R) + \frac{\sqrt{2}}{2} \frac{\mu}{v} \sin 2\theta_R$	0
$(1R, 2R)$	$\frac{1}{2} (\lambda_4 + \lambda_5 - \lambda_6) \sin 2\theta_R + \frac{\sqrt{2}}{2} \frac{\mu}{v} \cos 2\theta_R$	0
$(1I, 1I)$	$((\lambda_4 + \lambda_5) \cos^2 \theta_I + \lambda_6 \sin^2 \theta_I) - \frac{\sqrt{2}}{2} \frac{\mu}{v} \sin 2\theta_I$	0
$(2I, 2I)$	$((\lambda_4 + \lambda_5) \sin^2 \theta_I + \lambda_6 \cos^2 \theta_I) + \frac{\sqrt{2}}{2} \frac{\mu}{v} \sin 2\theta_I$	0
$(1I, 2I)$	$\frac{1}{2} (\lambda_4 + \lambda_5 - \lambda_6) \sin 2\theta_I + \frac{\sqrt{2}}{2} \frac{\mu}{v} \cos 2\theta_I$	0
$(1R, 1I)$	0	$\cos \theta_R \cos \theta_I$
$(1R, 2I)$	0	$\cos \theta_R \sin \theta_I$
$(2R, 1I)$	0	$\sin \theta_R \cos \theta_I$
$(2R, 2I)$	0	$\sin \theta_R \sin \theta_I$

The cubic couplings for $h\zeta_a\zeta_b$ is given by $-ig_{ab}v$ with g_{ab} defined in the second column of Table 1. The decay rate for $h \rightarrow \zeta_a\zeta_b$ is given by

$$\Gamma(h \rightarrow \zeta_a\zeta_b) = \frac{1}{1 + \delta_{ab}} \frac{1}{16\pi} \frac{v^2}{m_h} |g_{ab}|^2 \lambda^{\frac{1}{2}} \left(1, \frac{m_a^2}{m_h^2}, \frac{m_b^2}{m_h^2} \right), \quad (92)$$

where

$$\lambda(x, y, z) = x^2 + y^2 + z^2 - 2(xy + yz + zx). \quad (93)$$

The $h\eta^+\eta^-$ coupling is simply $-i\lambda_4 v$ while the SM hhh self coupling is $-i\lambda_1 v$.

A.4 $Z\zeta_a\zeta_b$ Couplings

From the covariant derivative $(D_\mu\eta)^\dagger(D^\mu\eta)$, we have the following derivative couplings

$$\begin{aligned} \mathcal{L}_{\text{int}} \supset & i\frac{g}{2} \left[W^{\mu+} \left(\eta^- \overleftrightarrow{\partial}_\mu (\eta_R + i\eta_I) \right) + W^{\mu-} \left((\eta_R - i\eta_I) \overleftrightarrow{\partial}_\mu \eta^+ \right) \right] \\ & + ie \left(A^\mu + \left(\frac{c_{\theta_w}^2 - s_{\theta_w}^2}{2s_{\theta_w} c_{\theta_w}} \right) Z^\mu \right) \left(\eta^- \overleftrightarrow{\partial}_\mu \eta^+ \right) + \frac{g}{2c_{\theta_w}} Z^\mu \left(\eta_R \overleftrightarrow{\partial}_\mu \eta_I \right), \end{aligned} \quad (94)$$

where the fields $\eta_{R,I}$ are related to the physical fields ζ_{1R} , ζ_{2R} , ζ_{1I} and ζ_{2I} as $\eta_R = \cos \theta_R \zeta_{1R} + \sin \theta_R \zeta_{2R}$ and $\eta_I = \cos \theta_I \zeta_{1I} + \sin \theta_I \zeta_{2I}$. From the last term in Eq. (94), we get the vertex for $Z(\epsilon_\mu(k)) \rightarrow \zeta_a(p) \zeta_b(p')$ as $+(g/2c_{\theta_w})c_{ab}(p-p')_\mu$ with c_{ab} defined in the last column of Table 1. The decay rate for $Z \rightarrow \zeta_a \zeta_b$ is given by

$$\Gamma(Z \rightarrow \zeta_a \zeta_b) = \frac{\sqrt{2}}{48\pi} G_F m_Z^3 |c_{ab}|^2 \lambda^{\frac{3}{2}} \left(1, \frac{m_a^2}{m_Z^2}, \frac{m_b^2}{m_Z^2} \right). \quad (95)$$

A.5 Formulas for the ΔS and ΔT

The analytic expressions for ΔS and ΔT can be given in terms of Passarino-Veltman functions which have been calculated using the software packages FormCalc [48] and LoopTools [49]. The SM expressions for S and T have been subtracted properly, we give hereafter only the extra contributions ΔS and ΔT . We take as reference point the Higgs mass $m_h = 125$ GeV, $m_t = 173$ GeV and assume $\Delta U = 0$.

We have checked both analytically and numerically that ΔS and ΔT are UV finite and also independent of the renormalisation scale. In terms of the Passarino-Veltman functions A_0 and B_{00} , they are given by

$$\begin{aligned} \Delta S = & \frac{1}{\pi m_Z^2} (2c_W^2 s_W 2A_0[m_{\eta^\pm}^2] - \cos^2 \theta_I \sin^2 \theta_R B_{00}[0, m_{\zeta_{1I}}^2, m_{\zeta_{2R}}^2] \\ & + B_{00}[0, m_{\eta^\pm}^2, m_{\eta^\pm}^2] (1 - 2s_W^2)^2 - \cos^2 \theta_I \cos^2 \theta_R B_{00}[0, m_{\zeta_{1R}}^2, m_{\zeta_{1I}}^2] \\ & - \cos^2 \theta_R \sin^2 \theta_I B_{00}[0, m_{\zeta_{1R}}^2, m_{\zeta_{2I}}^2] - \sin^2 \theta_R \sin^2 \theta_I B_{00}[0, m_{\zeta_{2R}}^2, m_{\zeta_{2I}}^2] \\ & - B_{00}[m_Z^2, m_{\eta^\pm}^2, m_{\eta^\pm}^2] + \cos^2 \theta_I \sin^2 \theta_R B_{00}[m_Z^2, m_{\zeta_{1I}}^2, m_{\zeta_{2R}}^2] \\ & + \cos^2 \theta_I \cos^2 \theta_R B_{00}[m_Z^2, m_{\zeta_{1R}}^2, m_{\zeta_{1I}}^2] + \sin^2 \theta_I \cos^2 \theta_R B_{00}[m_Z^2, m_{\zeta_{1R}}^2, m_{\zeta_{2I}}^2] \\ & + \sin^2 \theta_I \sin^2 \theta_R B_{00}[m_Z^2, m_{\zeta_{2R}}^2, m_{\zeta_{2I}}^2]) , \end{aligned} \quad (96)$$

$$\begin{aligned}
\Delta T = & \frac{-1}{4\pi m_W^2 s_W^2} (2s_W^4 A_0[m_{\eta^\pm}^2] + \cos^2 \theta_I \sin^2 \theta_R B_{00}[0, m_{\zeta_{1I}}^2, m_{\zeta_{2R}}^2] - \\
& \cos^2 \theta_I B_{00}[0, m_{\eta^\pm}^2, m_{\zeta_{1I}}^2] - \sin^2 \theta_I B_{00}[0, m_{\eta^\pm}^2, m_{\zeta_{2I}}^2] \\
& + (1 - 4s_W^4) B_{00}[0, m_{\eta^\pm}^2, m_{\eta^\pm}^2] - \sin^2 \theta_R B_{00}[0, m_{\eta^\pm}^2, m_{\zeta_{2R}}^2] \\
& + \cos^2 \theta_R \cos^2 \theta_I B_{00}[0, m_{\zeta_{1R}}^2, m_{\zeta_{1I}}^2] + \cos^2 \theta_R \sin^2 \theta_I B_{00}[0, m_{\zeta_{1R}}^2, m_{\zeta_{2I}}^2] \\
& - \cos^2 \theta_R B_{00}[0, m_{\zeta_{1R}}^2, m_{\eta^\pm}^2] + \sin^2 \theta_I \sin^2 \theta_R B_{00}[0, m_{\zeta_{2R}}^2, m_{\zeta_{2I}}^2]) . \tag{97}
\end{aligned}$$

References

- [1] C. Boehm, D. Hooper, J. Silk, M. Casse and J. Paul, Phys. Rev. Lett. **92**, 101301 (2004) [astro-ph/0309686].
- [2] M. Cirelli, N. Fornengo and A. Strumia, Nucl. Phys. B **753**, 178 (2006) [hep-ph/0512090].
- [3] P. J. Fox and E. Poppitz, Phys. Rev. D **79**, 083528 (2009) [arXiv:0811.0399 [hep-ph]].
- [4] L. Goodenough and D. Hooper, arXiv:0910.2998 [hep-ph].
- [5] T. E. Jeltema and S. Profumo, Mon. Not. Roy. Astron. Soc. **450**, no. 2, 2143 (2015) [arXiv:1408.1699 [astro-ph.HE]].
- [6] G. Bertone, D. Hooper and J. Silk, Phys. Rept. **405**, 279 (2005) [hep-ph/0404175].
- [7] C. Boehm, P. Fayet and R. Schaeffer, Phys. Lett. B **518**, 8 (2001) [astro-ph/0012504].
- [8] C. Boehm and R. Schaeffer, Astron. Astrophys. **438**, 419 (2005) [astro-ph/0410591].
- [9] C. Boehm, A. Riazuelo, S. H. Hansen and R. Schaeffer, Phys. Rev. D **66**, 083505 (2002) [astro-ph/0112522].

- [10] K. Sigurdson and M. Kamionkowski, Phys. Rev. Lett. **92**, 171302 (2004) [astro-ph/0311486].
- [11] G. Mangano, A. Melchiorri, P. Serra, A. Cooray and M. Kamionkowski, Phys. Rev. D **74**, 043517 (2006) [astro-ph/0606190].
- [12] S. Hannestad, R. S. Hansen and T. Tram, Phys. Rev. Lett. **112**, no. 3, 031802 (2014) [arXiv:1310.5926 [astro-ph.CO]].
- [13] X. Chu, B. Dasgupta and J. Kopp, JCAP **1510**, no. 10, 011 (2015) [arXiv:1505.02795 [hep-ph]].
- [14] A. Mirizzi, G. Mangano, O. Pisanti and N. Saviano, Phys. Rev. D **91**, no. 2, 025019 (2015) [arXiv:1410.1385 [hep-ph]].
- [15] M. S. Bilenky and A. Santamaria, hep-ph/9908272.
- [16] C. Boehm, J. A. Schewtschenko, R. J. Wilkinson, C. M. Baugh and S. Pascoli, Mon. Not. Roy. Astron. Soc. **445**, L31 (2014) [arXiv:1404.7012 [astro-ph.CO]].
- [17] J. A. Schewtschenko, R. J. Wilkinson, C. M. Baugh, C. Boehm and S. Pascoli, Mon. Not. Roy. Astron. Soc. **449**, no. 4, 3587 (2015) [arXiv:1412.4905 [astro-ph.CO]].
- [18] J. A. Schewtschenko, C. M. Baugh, R. J. Wilkinson, C. Boehm, S. Pascoli and T. Sawala, arXiv:1512.06774 [astro-ph.CO].
- [19] C. Boehm, Y. Farzan, T. Hambye, S. Palomares-Ruiz and S. Pascoli, Phys. Rev. D **77**, 043516 (2008) [hep-ph/0612228].
- [20] Y. Farzan, Phys. Rev. D **80** (2009) 073009 [arXiv:0908.3729 [hep-ph]].
- [21] Y. Farzan, S. Pascoli and M. A. Schmidt, JHEP **1010**, 111 (2010) [arXiv:1005.5323 [hep-ph]].

- [22] R. J. Wilkinson, C. Boehm and J. Lesgourgues, JCAP **1405**, 011 (2014) [arXiv:1401.7597 [astro-ph.CO]].
- [23] P. D. Serpico and G. G. Raffelt, Phys. Rev. D **70**, 043526 (2004) [astro-ph/0403417].
- [24] C. Boehm, M. J. Dolan and C. McCabe, JCAP **1212**, 027 (2012) [arXiv:1207.0497 [astro-ph.CO]].
- [25] C. Boehm, M. J. Dolan and C. McCabe, JCAP **1308**, 041 (2013) [arXiv:1303.6270 [hep-ph]].
- [26] K. M. Nollett and G. Steigman, Phys. Rev. D **91**, no. 8, 083505 (2015) [arXiv:1411.6005 [astro-ph.CO]].
- [27] E. Ma, Phys. Rev. **D73**, 077301 (2006).
- [28] N. G. Deshpande and E. Ma, Phys. Rev. **D18**, 2574 (1978).
- [29] For a recent update, see for example A. Arhrib, Y. L. S. Tsai, Q. Yuan and T. C. Yuan, JCAP **1406**, 030 (2014) [arXiv:1310.0358 [hep-ph]].
- [30] E. Ma, Phys. Lett. **B717**, 235 (2012).
- [31] G. Aad *et al.* (ATLAS Collaboration), Phys. Lett. **B716**, 1 (2012).
- [32] S. Chatrchyan *et al.* (CMS Collaboration), Phys. Lett. **B716**, 30 (2012).
- [33] E. Ma, Annales Fond. Broglie **31**, 285 (2006).
- [34] E. Ma, Phys. Rev. Lett. **86**, 2502 (2001) [hep-ph/0011121].
- [35] G. Aad *et al.* [ATLAS and CMS Collaborations], Phys. Rev. Lett. **114** (2015) 191803 [arXiv:1503.07589 [hep-ex]].

- [36] A. G. Akeroyd, A. Arhrib and E. M. Naimi, Phys. Lett. B **490**, 119 (2000) [hep-ph/0006035]; A. Arhrib, hep-ph/0012353.
- [37] G. Aad *et al.* [ATLAS Collaboration], JHEP **1601**, 172 (2016) [arXiv:1508.07869 [hep-ex]].
- [38] CMS Collaboration, CMS-PAS-HIG-15-012.
- [39] K. Cheung, J. S. Lee and P. -Y. Tseng, JHEP **1305**, 134 (2013) [arXiv:1302.3794 [hep-ph]]. G. Belanger, B. Dumont, U. Ellwanger, J. F. Gunion and S. Kraml, Phys. Rev. D **88**, 075008 (2013) [arXiv:1306.2941 [hep-ph]]. J. R. Espinosa, M. Muhlleitner, C. Grojean and M. Trott, JHEP **1209**, 126 (2012) [arXiv:1205.6790 [hep-ph]]; O. Lebedev, H. M. Lee and Y. Mambrini, Phys. Lett. B **707**, 570 (2012) [arXiv:1111.4482 [hep-ph]]; C. Englert, M. Spannowsky and C. Wymant, Phys. Lett. B **718**, 538 (2012) [arXiv:1209.0494 [hep-ph]].
- [40] K. A. Olive *et al.* [Particle Data Group Collaboration], Chin. Phys. C **38**, 090001 (2014).
- [41] M. E. Peskin and T. Takeuchi, Phys. Rev. D **46**, 381 (1992).
- [42] M. Baak *et al.* [Gfitter Group Collaboration], Eur. Phys. J. C **74** (2014) 3046 [arXiv:1407.3792 [hep-ph]].
- [43] G. Aad *et al.* [ATLAS Collaboration], arXiv:1507.04548 [hep-ex].
- [44] S. Dawson *et al.*, arXiv:1310.8361 [hep-ex]; D. Zeppenfeld, R. Kinnunen, A. Nikitenko and E. Richter-Was, Phys. Rev. D **62** (2000) 013009 [hep-ph/0002036];
- [45] C. Englert *et al.*, J. Phys. G **41** (2014) 113001 [arXiv:1403.7191 [hep-ph]]; G. Moortgat-Pick *et al.*, Eur. Phys. J. C **75**, no. 8, 371 (2015) doi:10.1140/epjc/s10052-015-3511-9 [arXiv:1504.01726 [hep-ph]].

- [46] A. Arhrib, R. Benbrik and N. Gaur, Phys. Rev. D **85**, 095021 (2012) [arXiv:1201.2644 [hep-ph]].
- [47] A. W. El Kaffas, W. Khater, O. M. Ogreid and P. Osland, Nucl. Phys. B **775**, 45 (2007) [hep-ph/0605142].
- [48] T. Hahn, Comput. Phys. Commun. **140**, 418 (2001); T. Hahn, C. Schappacher, Comput. Phys. Commun. **143**, 54 (2002); T. Hahn and M. Perez-Victoria, Comput. Phys. Commun. **118**, 153 (1999).
- [49] G. J. van Oldenborgh, Comput. Phys. Commun. **66**, 1 (1991); T. Hahn, Acta Phys. Polon. B **30**, 3469 (1999), PoS ACAT **2010**, 078 (2010) [arXiv:1006.2231 [hep-ph]].